Experimental research of sandwich specimens' failure mechanisms with facing layers from unidirectional fiber reinforced plastic with [0°] lay-up under axial compression

V. Paimushin[1,2*], *S.* Kholmogorov[1] and *M.* Makarov[1,2]

[1]Kazan National Research Technical University named after A. N. Tupolev – KAI, 10, K.Marx St., 420111 Kazan, Russia
[2] Kazan Federal University, 18, st. Kremlyevskaya, 420008 Kazan, Russia

Abstract. An experimental technique for compression tests of the sandwich specimens with thin outer layers made of fiber reinforced composite is proposed. The proposed method is focused on testing thin layers of composite material, specimens of which, even with a very short gage length, lose their stability, thereby distorting the determined value of the ultimate stress. Experimental studies of the failure mechanism of sandwich specimens with outer layers with $[0^o]$ lay-up under axial compression have been carried out. The possibility of realizing the shear buckling mode for specimens with different geometric parameters was revealed, which allows the determined ultimate stress formed in the outer layers to be taken as a mechanical characteristic when calculating the strength of structures made of composite materials. It is shown that for specimens with a honeycomb core in the outer layers under compression, an in-phase flexural buckling mode occurs. The implementation of a non-classical shear buckling mode is possible only for specimens with a rigid core, which was used as balsa wood.

1 Introduction

Sandwich structures are widely used in the shipbuilding and aerospace industries. As a rule, such constructions consist of two rigid outer layers, recieving tangential stresses, and a relatively low-rigid core, recieving transverse compression stresses and transverse shear stresses. The choice of materials for the outer layers and core depends on the specifics of the work of sandwich structures. In the aerospace industry, as a rule, honeycomb based on light aluminum alloys or polymer paper is used. Such cores have the highest stiffness and strength characteristics with a low weight. In sandwich structures used in shipbuilding, porous metal cores is used. Such cores require high toughness and high ability to absorb impact energy. Both metals and composite materials based on glass and carbon plastics are used as materials for the facing layers.

* Corresponding author: vpajmuhin@mail.ru

The failure of sandwich structures can be caused by the implementation of different processes of deformation of their constituent elements under the loading [1-4]: failure of the core due to the reaching of ultimate transverse shear stresses formed in them [5,6], fatigue fractures of the core [3,7]; peeling of the facing layers from the core [8,9]; reaching of ultimate transverse compressive stresses in the core [10]; buckling of the facing layers [11,12].

In ultralight sandwich structures, the outer layers are usually made of carbon fiber reinforced plastic (CFRP). Unidirectional carbon plastics can have even greater tensile strength than high strength steels. Therefore, the main failure reason of such structures may be the buckling of the facing layers in one form or another under the conditions of compressive stresses. In particular, in the formation of such stresses, it is possible to realize the transverse-shear buckling mode. As is known [13,14], when compressing specimens from unidirectional FRP along the fibers, the values of the transverse shear modulus can be taken as the ultimate compressive stresses. In a series of works [15, 16], it was shown that the theoretical identification of the shear buckling form of composite specimens under three-point bending conditions is possible using equations based on the simple kinematic model of S. P. Timoshenko.

In accordance with existing domestic and international standards, one of the types of CFRP specimens test is axial compression. For their implementation, as a rule, flat specimens with $[0^o]_s$, $[90^o]_s$ and $[\pm 45^o]_{2s}$ lay-up (s is the number laminas) are made. Even with a significant number of s, axial compression tests of specimens is accompanied by longitudinal-transverse bending, which affects the results of experimental studies. To reduce this phenomenon, it is possible to produce special composite specimens with a sandwich structure through the thickness, in which the outer layers are made of CFRP, and the middle layer, called a core, of a material whose mechanical characteristics are significantly lower in comparison with the mechanical characteristics of CFRP.

It is known that in compression tests of standard specimens made of FRP with a $[0^o]_s$ lay-up, the determined ultimate stress can be taken equal to the shear modulus [13,14,16], upon reaching which the failure of the FRP is due to the realization in it of the transverse shear buckling mode. To identify such buckling, a refined geometrically nonlinear theory of deformation of sandwich plates and shells with a transversely flexible core and outer layers made of composite was constructed in [17]. The refined shear model by S.P. Tymoshenko was used for the outer layers, taking into account the transverse compression. For the core, the three-dimensional equations of the theory of elasticity were integrated through the thickness, taking into account the equality of the tangential normal stresses to zero, and unknown tangential forces constant along the thickness were introduced. As shown by the results of the analytical solution of four-point bending problem of three-layer long test specimens, the equations constructed in [17] make it possible to reveal the shear buckling mode, which, as is known [18], are occurs in FRP with $G \ll E$ under compressive stresses.

To verify the results of the analytical solution obtained in [17], in [19], experimental studies of sandwich specimens failure with outer layers made of CFRP based on ELUR-P unidirectional carbon tape and cold-curing binder KhT-118 were carried out. It was shown that when using a polymer paper core in sandwich specimens, the implementation of the shear buckling mode is impossible. It is occurs only when using a rigid core – balsa wood, which was used in the manufacture of specimens in experiments.

2 Specimens and manufacture

In development of the results obtained in [16,19], in this work experimental studies of the failure mechanism of sandwich specimens with outer layers made of a unidirectional CFRP

under the axial compression were carried out. The main goal of the work is to identify the possibility of realizing the shear buckling mode for spesicmens with different geometric parameters, which allows to determine ultimate compressive stresses σ_*^-, formed in the outer layers to be taken as a mechanical characteristic when calculating structures made of composite materials.

For the experiments, four types of the following specimens were made: 1) $l = 35$ mm, $h = 5$ mm; 2) $l = 35$ mm, $h = 10$ mm; 3) $l = 50$ mm, $h = 10$ mm; 4) $l = 50$ mm, $h = 5$ mm with rigid core (l – gage length of the specimens, h – core thickness (Fig. 1)). The nominal thickness t of the outer layers was $2.00 - 2.40$ mm, the width b of all specimens was 20 mm. Specimens of type (1)–(3) were made with a honeycomb core, and for specimens of type (4) wood (balsa) was used as the core.

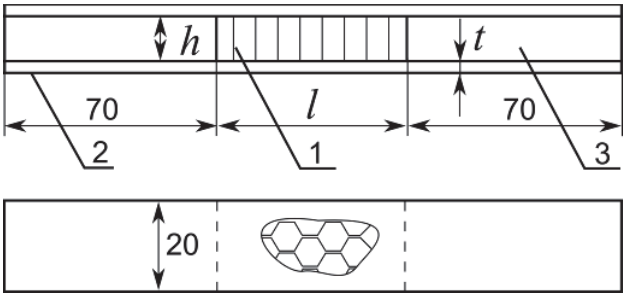

Fig. 1. Geometrical parameters of specimens: 1 – honeycomb core; 2 – FRP outer layers; 3 – embedded elements for clamp.

The outer layers of the specimens were made by vacuum molding. To do this, 17 laminas of ELUR-P carbon unidirectional tape were alternately impregnated with the KhT-118 binder, laid on a metal plate, which was covered with an airtight material, and then air was pumped out from it. The blanks for the outer layers were kept under vacuum for 24 hours, during which the binder was completely polymerized. After that, on the inner side of one of the blanks, in accordance with the sketch in Fig. 1, a honeycomb core and embedded parts made of fiberglass were laid, and the second blank was laid on top. All parts were glued together with a pre-applied binder. After the manufacture of a three-layer panel, specimens were cut from it with a diamond disk.

To apply a compressive axial load, the ASTM D3410 test fixture was used. It includes upper and lower wedge grips, which are interconnected by rigid guides. The compressive force was transmitted to the specimen by applying tangential forces to the gripping part of the specimen due to the self-tightening of the wedge grips.

3 Experimental results

In Fig. 2, we can see a sandwich specimen of type 2) installed in a test fixture.

Specimens with $l = 35$ mm, $h = 5$ mm. Table 1 shows the test results of four specimens of type 1) with a honeycomb thickness of $h = 5$ mm. The average ultimate compressive stress σ_*^- was found to be equal to $\sigma_*^- = 290$ MPa.

Table 1. Test results of four specimens with $l = 35$ mm, $h = 5$ mm.

	Width. mm	**Outer layer thickness. mm**	**Ultimate load. kN**	**Ultimate stress. MPa**
1	20.00	2.30	11.034	239.869
2	20.00	2.30	11.814	256.828
3	20.00	2.30	14.689	319.329
4	20.00	2.30	15.876	345.136
Average	**20.00**	**2.30**	**13.353**	**290.291**

Figure 3 shows the stress-strain diagrams of both outer layers of the fourth specimen (Table 1), obtained using strain gauges. It is seen that the diagrams can be considered linear up to failure strain $\varepsilon \approx 2000\mu$. On the diagrams, it is possible to accurately mark the moment of the beginning of the failure of the outer layers, characterized by a sharp increase in the difference of strains at a stress of $\sigma^{-} = 290$ MPa.

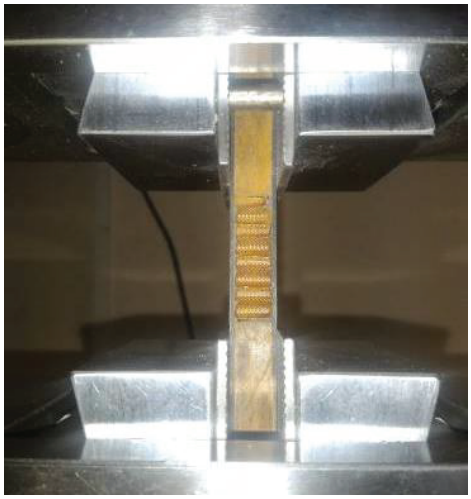

Fig. 2. Sandwich specimen in test fixture.

Despite the fact that the ultimate stresses for the fourth sample turned out to be equal to $\sigma_{*}^{-} = 345$ MPa, the diagrams were cut off at the value of $\sigma^{-} = 290$ MPa, since at that moment the strain gauges were destroyed and the strain data were incorrect. Figure 4 shows a curve of the difference between the strains of the outer layers, the values of which are calculated by the formula $\varepsilon_i^b = (\varepsilon_i^{(1)} - \varepsilon_i^{(2)})/(\varepsilon_i^{(1)} + \varepsilon_i^{(2)})$. It can be noted that in the range the strain difference is 5-10%. Based on the data obtained, it can be concluded that axial strain that are practically identical (with the specified degree of accuracy) in terms of magnitude are formed in the outer layers before failure.

From the analysis of the failure pattern (Fig. 5), it can be concluded that both outer layers retained their straightness, and the loss of bearing capacity occurred due to the shear buckling mode of the outer layer. The shear zone can be clearly observed at the top of the gage length of the specimen. The absence of bending is also indicated by the stress-strain diagrams in Fig. 3, in which there is no strain difference before failure.

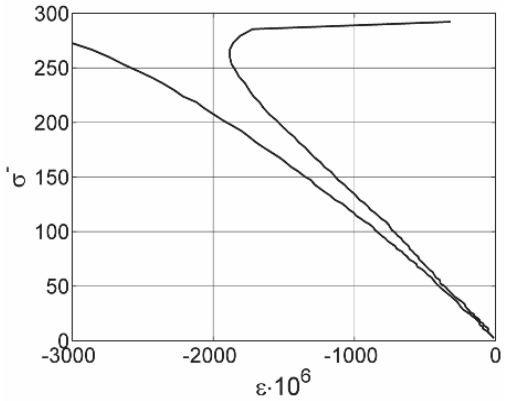

Fig. 3. Stress-strain diagram of two outer layers of specimen No. 4 $l = 35$ mm, $h = 5$ mm (MPa).

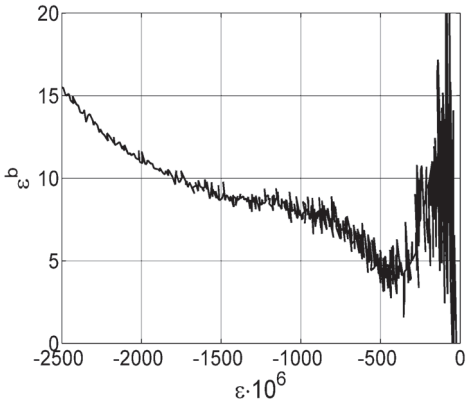

Fig. 4. Strain difference of outer layers for specimen No. 4 (%).

Fig. 5. Failure pattern of specimen ($l = 35$ mm, $h = 5$ mm).

Specimens with $l = 35$ mm, $h = 10$ mm. Table 2 contains the test results of four sandwich specimens. The value of the ultimate stress averaged over four specimens turned out to be equal to $\left\langle \sigma_*^- \right\rangle = 302$ MPa, and it agrees with a good degree of accuracy with the value for specimens of type 1).

Table 2. Test results of four specimens with $l = 35$ mm, $h = 10$ mm.

	Width. mm	**Outer layer thickness. mm**	**Ultimate load. kN**	**Ultimate stress. MPa**
1	20.00	2.40	17.130	356.875
2	20.00	2.40	15.589	324.771
3	20.00	2.40	11.264	234.667
4	20.00	2.40	14.046	292.625
Average	**20.00**	**2.40**	**14.507**	**302.234**

The stress-strain diagrams on the Fig. 6 characterize the deformation of the third sample from table 2. The nature of the diagrams is also identical to the diagrams in Fig. 3 for specimen No. 4: when the ultimate stress is reached, a sharp increase in the value ε_i^b from an almost zero value to 30% occurs, which can be observed in the dependence of Fig. 7.

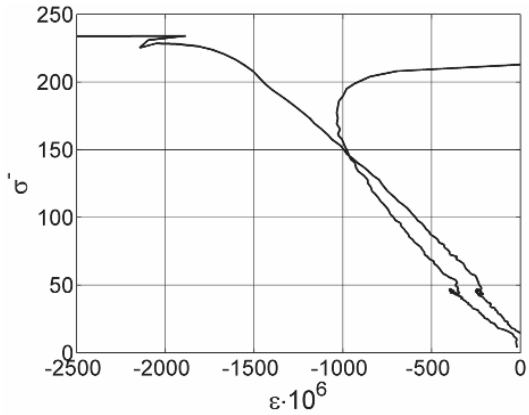

Fig. 6. Stress-strain diagram of two outer layers of specimen No. 3 $l = 35$ mm, $h = 10$ mm (MPa).

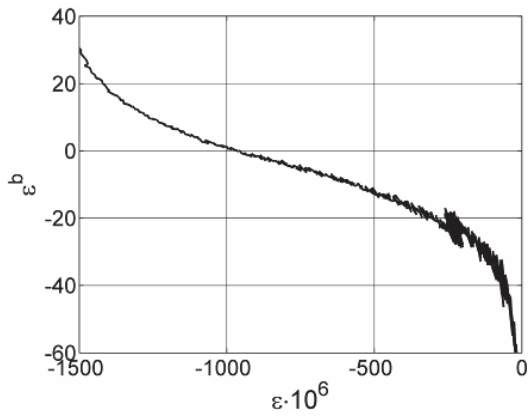

Fig. 7. Strain difference of outer layers for specimen No.3 (%).

Visual analysis of the failure pattern in Fig. 8 shows that one of the outer layers is destroyed in the lower part of gage length at the end of the gripping area, and the right layer has delamination. In the lower part of the gage length, on the right outer layer, one can notice a shear area, the formation of which, apparently, was the initiator of the failure.

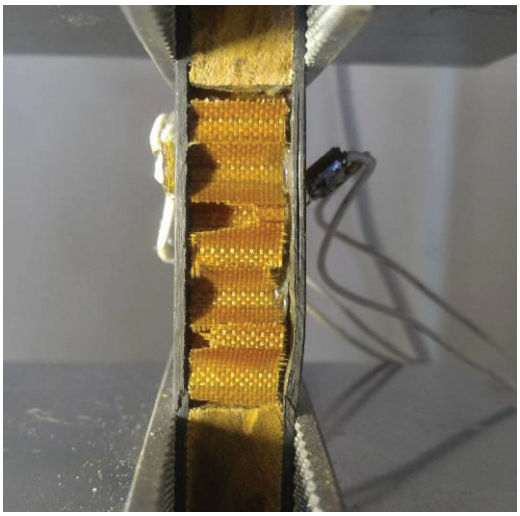

Fig. 8. Failure pattern of specimen ($l = 35$ mm, $h = 10$ mm).

Specimens with $l = 50$ mm, $h = 10$ mm. Two specimens were tested with an elongated gage length, the results are presented in table 3. The average critical ulitmate compressive stresses $\left\langle \sigma_*^- \right\rangle = 137$ MPa turned out to be significantly less than for specimens of types 1) and 2).

Table 3. Test results of four specimens with $l = 50$ mm, $h = 10$ mm.

	Width. mm	**Outer layer thickness. mm**	**Ultimate load. kN**	**Ultimate stress. MPa**
1	20.00	2.00	3.529	88.234
2	20.00	2.00	7.440	186.000
Average	**20.00**	**2.00**	**5.485**	**137.117**

An explanation for this can be obtained by analyzing the stress-strain diagrams of specimen No. 2 in Fig. 9: ultimate strain during failure reach values $\varepsilon \approx 700\mu$ that are much lower than for specimens of types 1) and 2). Bending strain throughout the deformation process until the moment of fracture are about 10 % (Fig. 10). A visual analysis of the deformation pattern on the Fig. 11 shows that the gage length loses its stability in the bending in-phase shape with the formation of one half-wave.

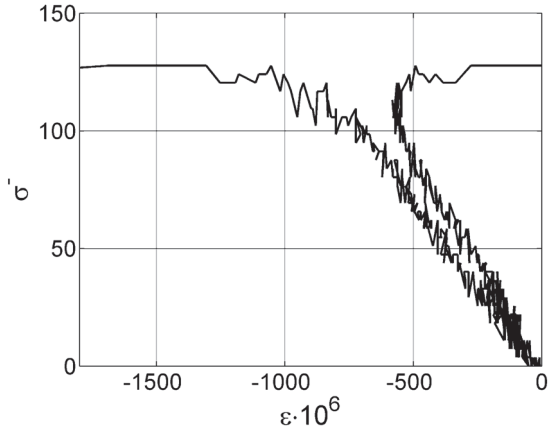

Fig. 9. Stress-strain diagram of two outer layers of specimen No. 2 $l = 50$ mm, $h = 10$ mm (MPa).

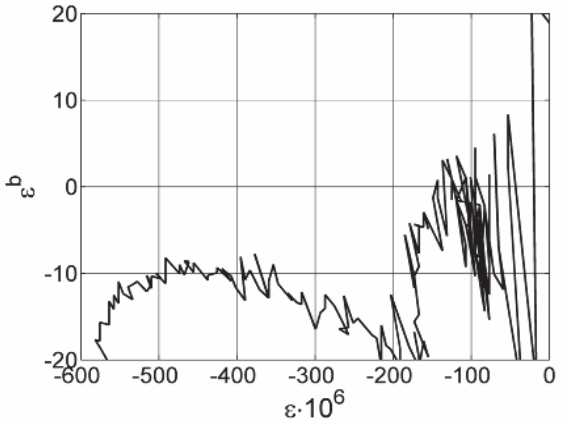

Fig. 10. Strain difference of outer layers for specimen No.2 (%).

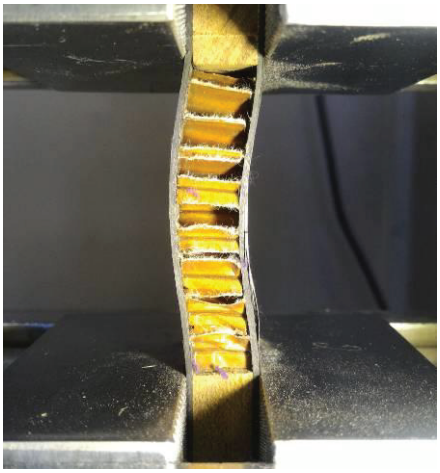

Fig. 11. Failure pattern of specimen ($l = 50$ mm, $h = 10$ mm).

Specimens with $l = 50$ mm, $h = 5$ mm and rigid core. In addition to specimens of type 3) with an long gage length, tests were carried out on specimens of type 4) with a rigid core

thickness of $h = 5$ mm, which was played by balsa wood. The test results are presented in table 4. It should be noted that the ultimate average stress $\left\langle \sigma_*^- \right\rangle$ over two specimens turned out to be equal to $\left\langle \sigma_*^- \right\rangle = 417$ MPa, which is significantly higher than the ultimate stress for the previous three types of specimens.

Table 4. Test results of four specimens with $l = 50$ mm, $h = 5$ mm and rigid core.

	Width. mm	**Outer layer thickness. mm**	**Ultimate load. kN**	**Ultimate stress. MPa**
1	20.00	2.00	15.684	392.105
2	20.00	2.00	17.702	442.555
Average	**20.00**	**2.00**	**16.693**	**417.330**

In Fig. 12 it can be seen that the stress-strain diagrams are almost linear. The loss of loading capacity in this case occurs due to the failure of the core in the gripping area of the gage length. Figure 12 shows, how one of the layers continues to deform linearly, while the core and the second layer collapsed.

4 Conclusion and final remarks

Composite elements of units and assemblies of aerospace engineering, depending on the purpose, can be made with a thickness of 0.5 to 20-30 mm. For example, the thickness of the wall or flange of the spars of medium or heavy aircraft made of unidirectional laminated composite can reach 30 mm, and the thickness of the wing skin of a light aircraft or glider is only 0.5-1 mm. Such a difference in the thickness of products can also dictate the manufacturing technology: elements with a relatively small thickness can be laid out manually from prepreg, while elements with a thickness of more than 10-15 mm are preferable to be made by infusion or by injection. It can be assumed that the mechanical properties of fiber reinforced composites with different methods of manufacturing finished products may differ, and the methods for obtaining mechanical characteristics under compression should cover all thicknesses.

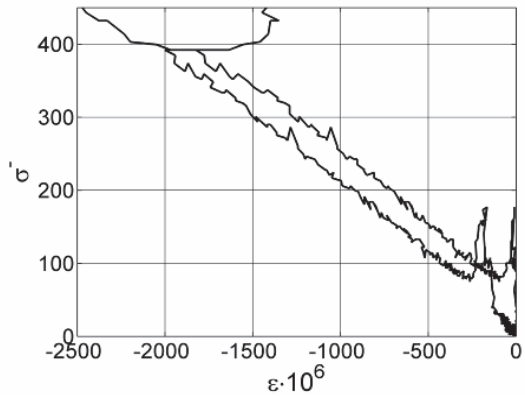

Fig. 12. Stress-strain diagram of two outer layers of specimen No. 1 $l = 50$ mm, $h = 5$ mm and rigid core (MPa).

The proposed method is focused on testing thin composite laminates, test specimens of which, even with a very short gage length, buckling, thereby distorting the determined value of the ultimate stress.

Table 5 presents the summary test results of all four types of specimens, as well as the results obtained on the basis of the analytical solution [20].

Table 5. Experimental results and analytical solution.

Specimen type	$\langle \sigma_*^- \rangle$, **MPa (experimental)**	σ_*^-, **MPa (analytical solution)**	
		σ_*^{in}	$\sigma_*^{ant}(n \to \infty)$
(1)	290	255	459
(2)	302	291	459
(3)	137	203	459
(4)	417	459	459
Four-point bending [20]	282	–	–

The ultimate stress σ_*^{in} in Table 5 corresponds to the in-phase buckling mode at $n = 1$ (n is the number of half-waves), and σ_*^{ant} to the transverse-shear buckling mode at $n \to \infty$. Analysis of the results shows that for specimens of types 1) – 3) the lowest ultimate stress correspond to in-phase buckling mode with $n = 1$, and for specimens of type 4) with a rigid core, the minimum critical stresses correspond to shear buckling mode. It can be noted that the experimental values $\langle \sigma_*^- \rangle$ of the ultimate compressive stresses for specimens (1)–(3) are slightly higher than the stresses σ_*^{in}, and for specimens of type (4) the stress values $\langle \sigma_*^- \rangle$ are closest to σ_*^{ant}.

Acknowledgements

This work was supported by the Russian Science Foundation (project No. 19-79-10018, Sect. 1, 3, 4) and by the Kazan Federal University Strategic Academic Leadership Program ("PRIORITY-2030", Sect. 2).

References

1. A. Petras, M.P.F. Sutcliffe, Composite Structures **44**, 237-252 (1999)
2. P. Rupp, P. Elsner, A. Weidenmann Kay, Journal of Sandwich Structures and Materials **21(8)**, 2654-2679 (2019)
3. H. Shi, W. Liu, H. Fang, Composites Part A: Applied Science and Manufacturing **109**, 564-577 (2018)
4. V.S. Sokolinsky, H. Shen, L. Vaikhanski, S.R. Nutt, Composite Structures **60**, 219-229 (2003)
5. J. Banghai, L. Zhibin, L. Fangyun, Composite Structures **133**, 739-745 (2015)
6. A. Fathi, F. Woff-Fabris, V. Altstadt, R. Gatzi, Journal of Sandwich Structures and Materials **15(5)**, 487-508 (2013)

7. F. Alila, J. Fajoui, R. Gerard, P. Casari, M. Kchaou, F. Jacquemin, Journal of Sandwich Structures and Materials **22(6)**, 2049-2074 (2018)
8. S. Piovar, E. Kormanikova, Advanced Materials Research **969**, 316-319 (2014)
9. A. Russo, B. Zuccarello, Composite Structures **81**, 575-586 (2007)
10. V. Crupi, G. Epasto, E. Guglielmino, Marine Structures **30**, 74-96 (2013)
11. V.N. Paimushin, M.V. Makarov, I.B. Badriev, S.A. Kholmogorov, Theory and Applications – Proceedings of the 11th international Conference **4**, 267-270 (2018)
12. I.B. Badriev, M.V. Makarov, V.N. Paimushin, Russian Mathematics **59(10)**, 57-60 (2015)
13. B. Budiansky, N.A. Fleck, Journal of the Mechanics and Physisc of Solids **41(1)**, 183-211 (1993)
14. A. Jumahat, C. Soutis, F.R. Jones, A. Hodzic, Composite Structures **92(2)**, 295–305 (2010)
15. V.N. Paimushin, D.V. Tarlakovskii, S.A. Kholmogorov, Uchenye Zapiski Kazanskogo Universiteta. Seriya Fiziko-Matematicheskie Nauki **158(3)**, 350–375 (2016)
16. V.N. Paimushin, S.A. Kholmogorov, M.V. Makarov et al, Angew Math Mech. **99(1)**, 1–25 (2018)
17. V.N. Paimushin, R.K. Gazizullin, N.V. Polyakova, M.A. Shishov, Advanced Structures Materials. Multiscale Solid Mechanics: strength, durability and dynamics **141**, 391-411 (2021)
18. A.N. Polilov, *Etudes on Mechanics of Composites* (Fizmatlit, M., 2015)
19. V.N. Paimushin, V.A. Firsov, S.A. Kholmogorov, M.V. Makarov, Advanced Structures Materials. Multiscale Solid Mechanics: strength, durability and dynamics **141**, 377–390 (2021)
20. V.N. Paimushin, M.V. Makarov, N.V. Polyakova, Mathematics **64(11)**, 83–89 (2020)